Monthly Notices of the ROYAL ASTRONOMICAL SOCIETY

MNRAS **513,** 1198–1209 (2022) https://doi.org/10.1093/mnras/stac800
Advance Access publication 2022 April 6

Helium line emissivities for nebular astrophysics

G. Del Zanna [1]★ and P. J. Storey[2]

[1]*DAMTP, Centre for Mathematical Sciences, University of Cambridge, Wilberforce Road, Cambridge CB3 0WA, UK*
[2]*Department of Physics and Astronomy, University College London, London WC1E 6BT, UK*

Accepted 2022 March 18. Received 2022 March 18; in original form 2022 January 25

ABSTRACT

We present the results of several collisional-radiative models describing optically thin emissivities of the main lines in neutral helium formed by recombination, for a grid of electron temperatures and densities, typical of H II regions and planetary nebulae. Accurate emissivities are required for example to measure the helium abundance in nebulae and as a consequence its primordial value. We compare our results with those obtained by previous models, finding significant differences, well above the target accuracy of 1 per cent. We discuss in some detail our chosen set of atomic rates and the differences with those adopted by previous models. The main differences lie in the treatment of electron and proton collision rates and we discuss which transitions are least sensitive to the choice of these rates and therefore best suited to high-precision abundance determinations. We have focused our comparisons on the case B approximation where only He and He^+ are considered, but also present results of full models including the bare nuclei, photoexcitation, and photoionization, and either black-body or observed illuminating spectrum in the case of the Orion nebula, to indicate which spectral lines are affected by opacity. For those transitions, accurate radiative transfer calculations should be performed. We provide tables of emissivities for all transitions within $n \leq 5$ and all those between the $n \leq 5$ and $n' \leq 25$ states, in the log T_e (K) $= 10^{3.0(0.1)4.6}$ and log N_e (cm^{-3}) $= 10^{2(0.5)6}$ ranges, and a FORTRAN code to interpolate to any T_e, N_e within these ranges.

Key words: atomic data – atomic processes – ISM: atoms – ISM: clouds – H II regions.

1 INTRODUCTION

Helium lines in the visible and near-infrared are particularly important for nebular astrophysics, for example being routinely used to measure the helium abundance in different astrophysical sources, and then extrapolating the results to obtain a measurement of its primordial abundance (see e.g. Peimbert, Luridiana & Peimbert 2007; Izotov, Thuan & Guseva 2014; Aver, Olive & Skillman 2015, and references therein). Such measurements are very important as they provide constraints on e.g. big bang nucleosynthesis models and galactic chemical evolution.

As spectral line intensities can be measured within an uncertainty of 1 per cent or so, a similar accuracy has been sought in atomic modelling. As we describe below, a significant effort was put in place by various groups to try to achieve such accuracy, by improving the modelling and the basic atomic rates. However, significant differences (up to 50 per cent or so) are found in the different calculations.

Recently, we constructed a new model for the level populations of, and resulting line emission from, helium in the relatively high-temperature, high-density plasma of the solar corona (Del Zanna et al. 2020). We reviewed the basic atomic rates and found some shortcomings in the rates adopted by previous authors. In this paper, we extend that model to predict helium line emissivities in the relatively low-temperature, low-density photoionized plasma typical of nebulae, and provide some comparisons with the previous models.

In the next section, we provide a brief overview of some of the most widely used previous models. In the following section, we present a summary of the rates adopted and the various atomic models we have built. A sample of results and comparisons with previous models is presented in Section 4, while Section 5 draws the conclusions.

2 PREVIOUS MODELS

Various models of helium emission in the conditions prevailing in photoionized plasma were developed in the 1950s and 1960s by several authors, including Mathis (1957), Seaton (1960), and Robbins (1970). Most of the early theory and methods adopted by subsequent authors are due to Seaton and Burgess, see e.g. Burgess & Seaton (1960a,b), Seaton (1962), and Pengelly & Seaton (1964).

The details of the various atomic models are not always entirely clear. However, we now summarize the main assumptions and rate coefficients adopted by the various authors.

The first detailed model of the He recombination spectrum is that of Brocklehurst (1972, B72). He built a model with the rates available at the time, and provided emissivities in the case A and B approximations (see Baker & Menzel 1938). For the l-changing collisional excitation (CE) rates, the semiclassical impact parameter approximation of Seaton (1962, S62) and Pengelly & Seaton (1964, PS64) was used. He used the non-degenerate formulation (S62, hereafter IP) for $l \leq 5$, and the degenerate formulation (PS64) for higher l. A few shortcomings in the model were pointed out by subsequent authors, the main one being that Brocklehurst (1972) neglected the metastability of the 2^3S, 2^1S states. The approach

★ E-mail: gd232@cam.ac.uk

was to solve the statistical balance equations in terms of departure coefficients b from Saha–Boltzmann level populations (the so-called b-factors). The calculations treated the singlet and triplet series separately and considered first n-resolved levels, b_n and then the b_{nl} for the terms (in *LS* coupling) were calculated for a lower set.

Almog & Netzer (1989, AN89) built a model with *LS* resolved states up to $n = 10$ (singlets) and $n = 12$ (triplets), and added four collapsed levels (Burgess & Summers 1969) to mimic the presence of levels up to $n = 100$, with the usual assumption that the collapsed states contain levels that are statistically populated. As the authors state, this model is a good assumption for high densities only, which was the main topic of that paper. Indeed collisional ionization was added into the model, as it is important for higher densities.

Smits (1996, S96) built an *LS* model, improving and correcting some errors in his previous models. Some details of the model can be found in Smits (1991, S91): many rates were calculated with the hydrogenic approximation. The method followed B72 and first calculated the b-factors for the n-resolved states up to $n = 496$. A matrix condensation technique (Burgess & Summers 1969) was employed to reduce the number of levels to 100. The b_{nl} factors were then calculated for a set of *LS*-resolved states up to $n = 50$ (2549 levels). The author then provided line emissivities calculated in case A and B for low densities, with the assumption that levels above $n = 50$ are statistically redistributed. As the author pointed out, this assumption is *not always valid*. The b_{nl} at $n = 50$ are not equal to the b_n for e.g. a density of 100 cm^{-3}. Smits argued that errors introduced by this assumption are not large, but without actually quantifying the statement. We will return to this issue below, as we have built several models and are able to assess this assumption.

S96 used for the $n \leq 9$ states the A-values obtained from the oscillator strengths calculated by Kono & Hattori (1984). For higher states, the Coulomb approximation was used for $l \leq 2$ states, and for the others a scaled hydrogenic approximation was adopted. CI rates were not included. The radiative recombination (RR) rate coefficients for lower n states were obtained from the OP photoionization (PI) cross-sections of Fernley, Seaton & Taylor (1987). For higher n, scaled hydrogenic rates were used. S91 states that CE rates within the $n = 2$, 3 levels are taken from the R-matrix calculations of Berrington & Kingston (1987, BK87). They were used to find the populations of the $n = 2$, 3 levels, to include the metastability of the 2s ^{3}S, which was not included by Brocklehurst (1972). The rest of the CE rates were taken from Brocklehurst (1972), i.e. using the impact parameter approximation. Smits (1996) noted that transfer of population between singlet and triplet states by electron collisions would be included if R-matrix CE rates for the lower states were used. This mixing was included in his model only for the $n = 2$ states. Spin–orbit and other relativistic interactions between ^{3}L$_L$ and ^{1}L$_L$ states for high L are also real effects not taken into account by Smits (1996). Both effects could reduce the populations of the triplets, compared to the singlets. However, Smits (1996) noted that comparisons with observations indicated an opposite trend, i.e. some of the predicted intensities of the triplets were lower than observations.

Drawing on the high-precision intermediate coupling variational calculations of helium structure and radiative processes by Drake (1996), Bauman et al. (2005) built an *LSJ* model of helium in the low-density limit (i.e. no collisions), and concluded that singlet–triplet mixing has a negligible effect on the total intensities of the lines within a multiplet. However, it is still unclear what effects collisional processes linking singlets and triplets have. As discussed below, we include these processes in our model up to $n = 5$ states. Bauman et al. (2005) also pointed out that individual intensities within a multiplet would be affected, but are generally not observable as line widths are larger than the separation of lines. A simpler *LS* model is therefore equivalent to an *LSJ* model.

Benjamin, Skillman & Smits (1999, B99) built a case B *LS* model with only the lower 29 states (up to $n = 5$), using the Sawey & Berrington (1993, SB93) R-matrix cross-sections for up to $n = 4$, with some interpolations and extrapolations. For the $n = 5$ states, IP rates for $l \leq 2$ and hydrogenic values for higher l were used. The A-values were mostly the same as in the S96 model, as well as the RR rates. For $\Delta n = 0$ and $n \geq 2$, CE rates for electrons, protons, and He$^+$ were included, using the IP method for low l and the PS64 otherwise, assuming equal proton and electron densities N, and $N(\mathrm{He}^+) = 0.1\,N$. For $\Delta n = 0$ and $n = 2$, the IP rates for collisions with protons and He$^+$ were included. For the CI, B99 included a rate for the 2^{3}S metastable level and the Vriens & Smeets (1980, VS80) semiclassical estimates for the other levels. The model built by B99 is much reduced in size compared to that presented by S96. To improve it, 'cascading' (described as an indirect recombination) contribution from the higher states was estimated so as to match the S96 populations within 2 per cent for densities lower than 10^6 cm^{-3}. However, as we show below, much larger differences between B99 and s96 are actually present in the line emissivities.

Porter et al. (2005, P05) constructed an *LS* model up to n^*, with an extra 'collapsed' $n^* + 1$ level describing the missing states between n^* and the continuum, and presented emissivities in the case B approximation. They noted that with $n^* = 100$, the corrections due to the collapsed level are negligible for low densities. Transition probabilities from the nearly exact calculations of Drake (1996) (up to $n = 10$) were used. PI cross-sections from Hummer & Storey (1998, HS98) were adopted to calculate the RR rates, while the CE rates of Bray et al. (2000) were used. For the l-changing collisions, they used the IP method of S62 for the s, p, and d states, and the semiclassical theory of Vrinceanu & Flannery (2001, VF01) for higher l.

Porter, Ferland & MacAdam (2007, P07) built a similar *LS* model up to $n = 40$, and added collapsed n-resolved levels between $n = 41$ and $n = 100$, i.e. similar to our coronal model for helium. They applied this model to study the helium abundance in the Orion nebula.

Porter et al. (2012, P12) presented an updated case B model, with the full set of HS98 PI cross-sections (up to $n = 25$) and associated RR rates. For higher n states, hydrogenic RR rates were used. The model included *LS* states up to $n = 100$, and a single collapsed $n = 101$ level. The paper reports that a code error in their earlier calculations (P05, P07) was uncovered, which affected mostly the 5876, 6678 Å lines, the decays from the singlet and triplet 3d levels. Fixing the code error mostly increased the recombination coefficients into the 3d levels. Other differences were due to a different implementation of the semiclassical Vriens & Smeets (1980) CE rates.

The P05, P07, and P12 models were built within the various improved versions of the He model within the CLOUDY (Ferland et al. 2017) photoionization code. The semiclassical theory of VF01 has been discussed by Guzmán et al. (2017) who show that due to the truncation of the cross-sections at energies that neglect the quantum mechanical tail, it grossly underestimates the collision rates, by a factor of six at $n = 30$, for example. Guzmán et al. (2017) also show that the PS64 method, on the other hand, gives rates close to those obtained from a quantum mechanical treatment.

Another point worth noting is that the IP proton rates as shown in Guzmán et al. (2017) and calculated within CLOUDY are also incorrect, as we noted in our coronal model paper (Del Zanna et al. 2020). We also found that the Bray et al. CE rate file in CLOUDY inverted by mistake the values for the transitions from the metastable 2s ^{3}S to the 4s ^{3}S and 4p ^{3}P (levels 12 and 14),

thus affecting somewhat the emissivities of the main decays from these two levels, the 3188 and 4713 Å lines. Thus, all the previous helium recombination models have apparent defects, in terms of using rates coefficients that are now considered not accurate or the best available at present. The purpose of this paper is therefore to investigate whether correcting these shortcomings has any impact on the emissivities of the spectroscopically important transitions.

3 MODELS

The present models are an extension of our previous coronal models described in Del Zanna et al. (2020). Among them, the most extended neutral He model for low-temperature ($T = 20\,000$ K) plasma was a set of *LS*-resolved states up to $n = 40$, and a set of n-resolved levels up to $n = 100$. Considering the behaviour of the b factors, this model was deemed sufficient for electron densities higher than $N = 10^6$ cm^{-3}.

For this paper, we have built a model for neutral He with *LS*-resolved states up to $n = 100$ and n-resolved levels up to $n = 500$. This is a much larger model than the previous ones, and especially larger than the largest model (*LS*-resolved states up to $n = 50$) produced by S91 and subsequently used by S96 and B99. For He$^+$, we adopted the *J*-resolved CHIANTI (Dere et al. 2019) model. We create a collisional-radiative model, with matrices that contain all the main rate coefficients affecting the bound levels, and obtain the level populations in equilibrium by direct inversion.

We did not include dielectronic recombination (DR), the key process in our coronal model, as it is negligible at the low temperatures of interest here. For RR and $L \leq 3$, we use rates obtained by numerical integration of the photoionization cross-sections calculated by Hummer & Storey (1998) in the *R*-matrix approximation with a target that accounted for the dipole and quadrupole polarizabilities of the He$^+$ ground state. Hummer & Storey (1998) showed that their calculated bound–free cross-sections agree within 1 per cent with the bound–bound radiative data of Drake (1996) when extrapolated to the series limit. Hydrogenic values were used for RR for $L > 3$.

For the *LS* levels up to $n = 10$, we have used the energies and A-values of Drake & Morton (2007). The energies for the higher levels were obtained from the quantum defects using the updated coefficients of Drake (2006). The A-values for the higher *LS* states were obtained either from fits to the results of Drake & Morton (2007), as described by Hummer & Storey (1998), or using the methods of Bates & Damgaard (1949) and van Regemorter, Binh Dy & Prudhomme (1979), and the hydrogenic approximation using the code RADZ1 (Storey & Hummer 1991). The A-values for the n-resolved states to the lower $n = 2$, 3 states were obtained from statistically weighted averages of the extrapolated Drake & Morton (2007) results. The A-values for the n-resolved states to the lower $n = 4$ up to 40 states were obtained by averaging hydrogenic values. The A-values between the n-resolved states were obtained as in our previous coronal model, using the hydrogenic analytical formulation and tabulated Gaunt factors.

For the electron CE rates of states up to $n = 5$, we use the *R*-matrix results of Bray et al. (2000), although we have also experimented with other rates. The lowest temperature for the Bray et al. (2000) rates is 5623 K. To provide estimates to lower temperatures, we have proceeded as follows. For the CE rates within the $n = 2$, 3 states, we have taken the *R*-matrix rates from BK87, which were calculated down to 1000 K. As some small differences between the two sets of rates are present, we have interpolated the BK87 rates to 5623 K, and scaled them so they agree at this temperature with the Bray et al. values. For the $n = 4$ states, we have scaled the SB93 rates in a similar way, and then extrapolated them down to 1000 K in the Burgess & Tully (1992) scaled domain, with a linear fit to the first two points (SB93 CE rates were calculated for 2000 and 5000 K). For the $n = 5$ states, we have linearly extrapolated the Bray et al. CE rates in the Burgess and Tully scaled domain, considering again the first two points. The CE rates were stored in the scaled domain, where the interpolation in temperature is carried out, as done within the CHIANTI software.

Note that the collision strength calculations of Sawey & Berrington (1993) and of Bray et al. (2000) both employ the *R*-matrix method but the latter calculation is to be preferred because it makes allowance for the presence of continuum target states with the result that their collision rates between bound states are almost always smaller than those of Sawey & Berrington (1993) due to flux lost to the continuum states. It should be noted, however, that the allowance for continuum states gives rise to some resonance features near threshold that, although they represent a physical process, are not necessarily correct in detail. Thus a measure of uncertainty is still attached to the CE between low-lying states that is difficult to quantify. Finally, we point out that extrapolating the rates to temperatures lower than 1000 K is feasible but the values would be quite uncertain.

To connect the states with $n \leq 5$ to higher states, $m > 5$, we extrapolated the cross-sections of Bray et al. (2000) for $n < m \leq 5$ assuming they vary as m^{-3}. Attempts to directly calculate CE rates to the higher levels proved unreliable, as discussed in Del Zanna et al. (2020). For the other states, we used the IP method for $\Delta n = 1$ transitions. For $\Delta n = 2$, 3, 4 transitions within the n-resolved levels, we adopted the Percival & Richards (1978) approximation.

For the l-changing ($\Delta n = 0$, $\Delta l = 1$) collisions for electrons and protons we used the IP approximation among the non-degenerate levels with lower l and the Pengelly & Seaton (1964, PS64) for the remainder. The switching was applied when the difference in energy reached 10^{-4} cm^{-1}. We note that an improved PS64 method has been developed by Badnell et al. (2021). We have checked that differences with the PS64 rates are negligible. We assumed a fixed proton to electron number ratio of 0.91, which results from assuming that the helium abundance is 10 per cent by number that of hydrogen.

We included collisional ionization (CI) and three-body recombination as described in our previous model for the lowest states, but use the semiclassical CI rates of Vriens & Smeets (1980) instead of those developed by A. Burgess (ECIP). We recalculated the rates for the low temperatures considered here. We note that CI has a negligible effect at the low densities considered here, as the model is driven by photoionization (PI) and resulting RR cascading. For the PI cross-sections, we have used the Hummer & Storey (1998) results, instead of the semiclassical Kramers hydrogenic formula and the Gaunt factors from Karzas & Latter (1961) as in our previous paper. The key factors are the RR rates, the CE rates within the lower levels (for higher densities), the set of A-values, and the cascading effects from the higher to the lower states. Further details on other specific rates are given in Del Zanna et al. (2020).

The emissivities are defined as

$$E = \frac{4\,\pi\, j}{N_{\rm e}\, N({\rm He}^+)} = \frac{h\,\nu_{ji}\, N_j\, A_{ji}\, N({\rm He})}{N_{\rm e}\, N({\rm He}^+)} \quad {\rm erg\,cm^3\,s^{-1}}, \tag{1}$$

where the first definition is how the emissivities are usually indicated in the literature, and the second one is how we calculated them: N_j is the population of the upper level j, relative to the total population of He, N(He), i.e. He^0 and He$^+$; A_{ji} is the radiative transition probability, and $h\,\nu_{ji}$ is the energy of the photon.

We calculate the emissivities in case A (optically thin plasma) and case B, which is an approximation to model the real plasma emission when the strongest singlet lines, decaying to the ground state, are re-absorbed on the spot. To obtain case B, we have set to zero the RR

to the ground state and all the A-values of the singlet (above $n = 2$) decays to the ground state.

Clearly, detailed modelling allowing for radiative transfer of line and continuum photons is needed to study specific sources. Here, we are mostly interested in showing how line emissivities are affected by the use of different models and atomic rates.

Our general model includes all three ionization stages of He but to make a direct comparison to earlier tabulated emissivities, we make the simplifying assumption adopted in previous models, where only neutral He and He^+ (and not the bare nuclei) are considered, to mimic the conditions in the He^+ zone of a photoionized nebula. Various options are available to achieve this, forcing the relative numbers of neutral He and He^+, for example using a 'laser' monoenergetic photon source (Ferland, private communication). In a similar way, we construct the present case B model (PB in the emissivity tables), in which we include a dilute black-body radiation field with $T = 100\,000$ K, which is used to photoionize only the ground state. The function of this field is to establish a physically reasonable He^+ fraction and a range of choices of temperature and dilution factor are possible that have this effect. Parameters were chosen that approximate the conditions in a planetary nebula surrounding a hot white dwarf. We also removed the photons below 228 Å, which would normally be absorbed in ionizing He^+ closer to the ionizing star and not present in the zone where the He recombination spectrum is formed. In this model, we do not include photoexcitation (PE) effects, as also assumed in earlier work on the case B helium recombination spectrum. In this way, the emissivities are independent of the chosen dilution factor.

To assess how reliable a reduced model (similar to that of S96) is for nebular densities, we had initially considered the earlier coronal model, with *LS*-resolved states up to $n = 40$ and n-states up to $n = 100$. However, for the lowest densities considered here (10^2 cm^{-3}), we found that the b-factors reach unity only around $n = 200$, so we have therefore built a new model, which we call PB40, with *LS*-resolved states up to $n = 40$ and n-states up to $n = 300$. The rates for this model are essentially the same as those of the full $n = 500$ model. We used the same black-body flux to photoionize the ground state to establish a reasonable ionization balance. Also, to show the effects that different CE rates can have, we have also modified the PB40 model by replacing the Bray et al. CE rates with those from Sawey & Berrington (1993) for states up to $n = 4$, and IP rates for the $n = 5$ levels, to approximate the rates used by B99 (although some differences are present). We call this model SB93.

Finally, we have also built another case B model (which we call PB + PE + PI) where we have considered the level balance between He, He^+, and He^{++} still using the same black-body flux, and including both PI and PE. Photoexcitation (and de-excitation) was included for all allowed transitions. PI was included for all states up to $n = 25$ using the PI cross sections from Hummer & Storey (1998), although we note that only those for the ground state and the metastable are relevant here. These cross-sections are close (within a few per cent) of those in TOPBASE. The photon energies have been adjusted to the observed thresholds. As shown below, for sufficiently low dilutions, the results of this model are close to those of the PB model.

4 RESULTS

We present a sample of results, for a temperature $T = 10\,000$ K and three electron densities, $N = 10^6$, 10^4, 10^2 cm^{-3}. Fig. 1 shows the b factors obtained from the model PB, *LS*-resolved states up to $n = 100$ and n-resolved levels up to $n = 500$ in case B. b factors only up

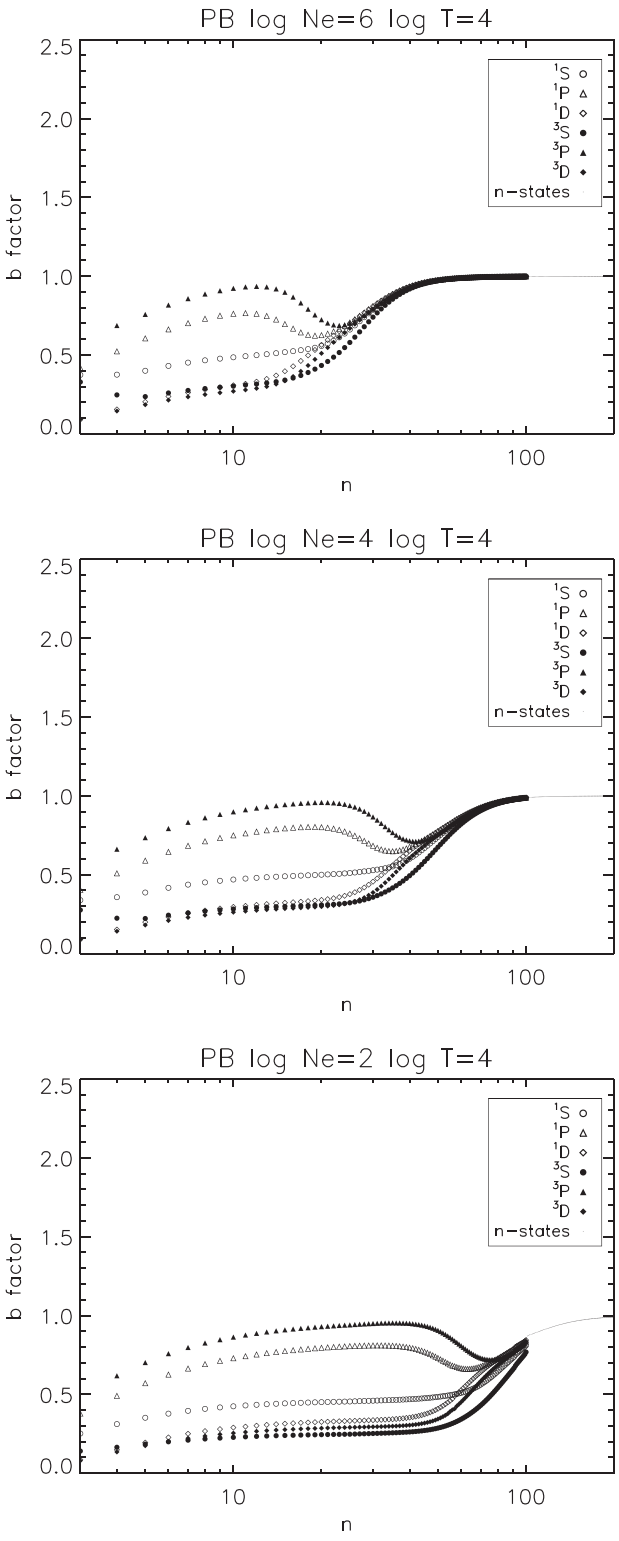

Figure 1. b factors obtained with our full case B model, *LS*-resolved states up to $n = 100$ and n-resolved levels up to $n = 500$. Only values up to $n = 200$ are shown.

Table 1. Emissivities (10^{-26} erg cm^3 s^{-1}) of the strongest He lines, for $T_e = 10\,000$ K and $N_e = 10^2$ cm^{-3} in case B.

λ (Å)	Levels	Earlier work					Present work			
		B72	S96	B99	P05	P12	SB93	PB40	PB	PB + PI + PE
2945	T 5p-2s	2.66	–	2.70	2.69	2.70	2.71	2.71	2.70	2.70
3188	T 4p-2s	5.55	5.61	5.62	5.62	5.62	5.62	5.62	5.61	5.61
3889	T 3p-2s	13.7	13.6	13.7	14.1	14.0	14.0	14.0	14.0	14.0
3965	S 4p-2s	–	1.39	1.39	1.41	1.42	1.42	1.42	1.41	1.41
4026	T 5d-2p	2.87	2.86	2.86	2.92	2.91	2.91	2.91	2.91	2.91
4388	S 5d-2p	–	0.76	0.76	0.77	0.77	0.77	0.77	0.77	0.77
4471	T 4d-2p	6.05	6.15	6.16	6.12	6.12	6.13	6.12	6.12	6.13
4713	T 4s-2p	0.56	0.63	0.65	0.65	0.64	0.65	0.65	0.65	0.65
4922	S 4d-2p	–	1.63	1.64	1.66	1.65	1.65	1.65	1.63	1.65
5016	S 3p-2s	–	3.48	3.49	3.54	3.56	3.55	3.55	3.55	3.55
5876	T 3d-2p	16.7	16.8	18.90	16.3	16.9	16.9	16.9	17.0	17.0
6678	S 3d-2p	–	4.78	4.79	4.63	4.80	4.80	4.80	4.83	4.83
7065	T 3s-2p	2.0	2.83	2.96	3.0	2.98	2.99	2.99	2.98	2.98
7281	S 3s-2p	–	0.89	0.90	0.89	0.90	0.90	0.90	0.90	0.90
10830	T 2p-2s	26.8	34.3	34.0	33.2	33.4	33.8	33.5	33.5	33.6
18685	T 4f-3d	–	–	2.22	2.18	2.20	2.21	2.21	2.24	2.23
20587	S 2p-2s	–	4.12	4.13	–	4.15	4.17	4.16	4.17	4.17

Note. The first column gives the wavelength (in air, except the last ones in vacuum), the second indicates if a line is between singlets (S) or triplets (T). B72: Brocklehurst (1972), S96: Smits (1996), B99: Benjamin et al. (1999), P05: Porter et al. (2005), P12: Porter et al. (2012), SB93: $n = 40$ model with the SB93 rates; PB40: $n = 40$; PB: full $n = 500$; PB + PI + PE: full $n = 500$ model with PI and PE and dilution $d = 10^{-16}$.

Table 2. Emissivities (10^{-26} erg cm^3 s^{-1}) of the strongest He lines, for $T_e = 10\,000$ K and $N_e = 10^4$ cm^{-3} in case B.

λ (Å)	Levels	Earlier work					Present work			
		B72	S96	B99	P05	P12	SB93	PB40	PB	PB + PI + PE
2945	T 5p-2s	2.67	–	2.73	2.82	2.84	2.83	2.83	2.83	2.83
3188	T 4p-2s	5.57	5.63	6.07	6.12	6.12	6.13	6.01	6.01	6.01
3889	T 3p-2s	13.7	13.7	16.7	16.8	16.6	17.0	16.7	16.7	16.7
3965	S 4p-2s	1.42	1.39	1.43	1.47	1.51	1.47	1.47	1.47	1.47
4026	T 5d-2p	2.88	2.87	2.87	3.03	3.02	3.02	3.02	3.02	3.02
4388	S 5d-2p	0.78	0.76	0.76	0.80	0.81	0.79	0.79	0.79	0.79
4471	T 4d-2p	6.07	6.16	6.52	6.47	6.46	6.57	6.43	6.44	6.44
4713	T 4s-2p	0.56	0.63	0.95	0.83	0.82	0.95	0.89	0.88	0.88
4922	S 4d-2p	1.66	1.64	1.69	1.72	1.77	1.71	1.70	1.70	1.70
5016	S 3p-2s	3.57	3.49	3.73	3.81	3.90	3.81	3.78	3.79	3.79
5876	T 3d-2p	16.8	16.7	19.1	18.7	19.4	19.3	19.1	19.1	19.1
6678	S 3d-2p	4.80	4.75	5.05	4.96	5.45	5.10	5.06	5.06	5.06
7065	T 3s-2p	1.99	2.84	6.15	5.90	5.82	6.06	5.88	5.87	5.89
7281	S 3s-2p	0.84	0.46	1.28	1.20	1.23	1.27	1.21	1.21	1.21
10830	T 2p-2s	26.8	234.4	204.7	188	185	196	188	188	189
18685	T 4f-3d	–	–	2.26	2.28	2.36	2.29	2.27	2.27	2.27
20587	S 2p-2s	–	6.91	6.75	–	6.73	6.70	6.60	6.60	6.61

to $n = 200$ are shown, as they have already reached near unity for $n = 100$. For example, at 10^2 cm^{-3}, the b factors are 0.9968 at $n = 200$ and 0.998 at $n = 300$. The figures indicate a smooth behaviour in transitioning from the *LS*-resolved to the n-resolved states. The assumption that the n-resolved states are in statistical equilibrium is validated.

The resulting emissivities for all the strongest He lines in the visible/near-infrared are shown in the last two columns of the emissivity Tables 1–3. Additional tables are provided in the Appendix. Our final results are in the penultimate column, designated PB. The final column displaying the effect of adding photoionization and photoexcitation of excited states will be discussed later.

The emissivities with the reduced $n = 40$ model (PB40) are also given in the tables. There is generally excellent agreement with the PB results, with the largest difference of 1.7 per cent for the lowest temperatures and densities. This largely confirms the suggestion by S91 that their model (which we recall was similar to our PB40 calculation in that it included *LS*-resolved states up to $n = 50$) would provide reasonably accurate emissivities even at 10^2 cm^{-3} for the most prominent optical lines.

Earlier results are shown in previous columns. Despite the simplified rates used in the first complete model built by Brocklehurst (1972), and the neglect of the metastability of the 2^3S, 2^1S states, relatively good agreement for many lines can be seen. We expected close agreement with the other models, but that is not the case. There are also surprising large differences for some lines between the S96 and B99 models, contrary to the B99 statement that agreement was present at the 2 per cent level.

We experimented with changing various rates, and found that at these plasma T_e, N_e the electron CE rates among the lower levels have a significant effect, as already pointed out in previous literature. The values of the CE rates are relatively uncertain compared to radiative rates, so we begin by comparing the different calculations

Table 3. Emissivities (10^{-26} erg cm^3 s^{-1}) of the strongest He lines, for $T_e = 10\,000$ K and $N_e = 10^6$ cm^{-3} in case B.

λ (Å)	Levels	Earlier work					Present work			
		B72	S96	B99	P05	P12	SB93	PB40	PB	PB + PI + PE
2945	T 5p-2s	2.72	–	2.79	2.96	2.97	2.92	2.92	2.92	2.92
3188	T 4p-2s	5.66	5.72	6.32	6.51	6.48	6.40	6.24	6.24	6.24
3889	T 3p-2s	14.0	13.9	17.9	18.3	18.1	18.3	17.9	17.9	17.9
3965	S 4p-2s	1.45	1.42	1.47	1.54	1.59	1.51	1.51	1.51	1.51
4026	T 5d-2p	2.93	2.89	2.89	3.18	3.14	3.09	3.09	3.09	3.09
4388	S 5d-2p	0.79	0.77	0.76	0.83	0.85	0.81	0.81	0.81	0.81
4471	T 4d-2p	6.15	6.20	6.70	6.81	6.76	6.78	6.60	6.60	6.60
4713	T 4s-2p	0.56	0.63	1.07	0.91	0.90	1.07	0.98	0.98	0.98
4922	S 4d-2p	1.68	1.65	1.73	1.80	1.85	1.75	1.73	1.73	1.73
5016	S 3p-2s	3.63	3.54	3.87	4.04	4.13	3.96	3.93	3.93	3.93
5876	T 3d-2p	16.8	16.6	19.9	20.2	20.85	20.1	19.9	19.9	19.9
6678	S 3d-2p	4.80	4.73	5.15	5.22	5.77	5.21	5.14	5.14	5.14
7065	T 3s-2p	2.0	2.86	7.34	7.17	7.00	7.25	7.00	7.00	7.00
7281	S 3s-2p	0.85	0.89	1.42	1.36	1.38	1.42	1.34	1.34	1.34
10830	T 2p-2s	27.1	320	267	255	247	259	247	247	247
18685	T 4f-3d	–	–	2.24	2.37	2.47	2.26	2.24	2.24	2.24
20587	S 2p-2s	–	8.54	8.15	–	8.25	8.09	7.97	7.97	7.97

at the lowest density, where CE is much less significant. At 10 000 K, we find average absolute differences of 1.6 per cent (maximum 5.0 per cent) compared to S96, 1.5 per cent (maximum 11.1 per cent) compared to B99, 1.1 per cent (maximum 4.1 per cent) compared to P05 and 0.45 per cent (maximum 1.8 per cent) compared to P12. All four of these calculations used highly accurate bound–bound radiative transition probabilities, although from different authors, and differ primarily in their treatment of radiative recombination. As in the current work, the results of P05 and P12 derive radiative recombination rates from the photoionization cross-sections of Hummer & Storey (1998), which are to be preferred to the Opacity Project cross-sections used by S96 and B99.

At typical nebular temperatures, CE from the ground state is negligible compared to recombination but excitation from the 2 ^{3}S metastable is significant as temperature and/or density increases. It is instructive to consider the emissivity of the 2 ^{3}P–2 ^{3}S λ10830 since it is excited by recombination and cascading through the triplet terms and also strongly affected by CE from the metastable. Similar but smaller effects of CE are seen for other low-lying triplets and to a much lesser extent, the singlet states. The λ10830 transition is also important because it is particularly useful in constraining the helium abundance, as shown e.g. by Izotov et al. (2014) and subsequent authors. The emissivities for λ10830 are summarized in Table 4 at three densities and three temperatures. The fuller tables of emissivities for temperatures of 5000K and 20 000K are in the appendix. The contribution of CE from the metastable 2 ^{3}S depends directly on the population in that state. At low densities it is populated primarily by recombination followed by radiative decay to the ground state and the population increases with increasing density but as the density increases collisional de-excitation to the ground state and CE to higher singlet states cause the population to plateau once collisional de-excitation dominates over radiative decay. The rising population of the metastable is reflected in the increasing emissivity of λ10830 with increasing density and temperature. The calculations of S96 and B99 used the effective collision strength data from Sawey & Berrington (1993) for this excitation process while P05, P12, and this work took effective collision strengths from Bray et al. (2000). To isolate the effect of only changing the choice of effective collision strength, we can compare the results of our PB40 model with a model using the Sawey & Berrington (1993) data (SB93) at 10 000K and at densities were CE of λ10830 is dominant. The

Table 4. Emissivities (10^{-26} erg cm^3 s^{-1}) of the λ10830 line as a function of temperature (T_e) electron density (N_e) in case B.

T (K)	Calc.	N_e (cm^{-3})		
		10^2	10^4	10^6
5000	PB	50.6	130	189
	P12	50.8	140	213
	P05	49.9	140	214
	B99	50.7	152	234
10 000	PB	33.5	188	247
	P12	33.4	185	247
	P05	33.2	188	255
	B99	34.0	205	267
	PB40	33.5	188	247
	SB93	33.8	196	259
20 000	PB	23.6	204	256
	P12	23.8	181	215
	P05	23.4	188	237
	B99	24.6	207	253

SB93 emissivities are larger by 4.3 per cent at density 10^4 cm^{-3} and 4.9 per cent at density 10^6 cm^{-3}. Sawey & Berrington (1993) and Bray et al. (2000) tabulate their effective collision strengths on different temperature grids which only coincide at 10 000K, where we find that the Sawey & Berrington (1993) effective collision strengths for the 2 ^{3}P–2 ^{3}S excitation is larger than that of Bray et al. (2000) by 4.2 per cent showing that changes to the collision strengths result in commensurate changes to the emissivity, as one might expect. Benjamin et al. (1999) used the Sawey & Berrington (1993) CE rates and their results agree better with our SB93 model than with PB40.

There are, however, significant differences between our final results and those of P12, even though we used the same CE rates of Bray et al. (2000). As noted above, agreement is very good at the lowest density where radiative processes dominate and CE is not significant but not at the higher densities for some temperatures. The exception is the temperature of 10^4 K where the P12 emissivity is 1.6 per cent lower than ours at 10^4 cm^{-3} and agrees within 0.4 per cent at 10^6 cm^{-3}. But at 5000 K, the differences are 7.7 per cent and

13.4 per cent at those densities, while at 20 000 K the differences are −11.7 per cent and −16.3 per cent. Bray et al. (2000) tabulate effective collision strengths on a logarithmic, base ten, mesh with interval 0.25 with the result that the temperature of 10 000 K is the only one of the three temperatures under discussion that corresponds to a tabulated value in their paper. The observation that P12 agrees well with the present results only at 10 000 K suggests that P12 have used a different approach to the interpolation of the tables of Bray et al. (2000) or have not used their results for all temperatures.

The features that we have seen when comparing our results to those of P12 for the 10830 Å transition are present in most transitions in the emissivity tables at 5000, 10 000, and 20 000 K. Agreement is good at the lowest density with average absolute differences of 1.3 per cent or less. With increasing density the differences become larger, reaching 5.5 per cent at 5000 K and 16.1 per cent at 20 000 K at density 10^6 cm^{-3}. These average differences conceal some very large individual differences between our work and P12. For example at 20000 K and a density of 10^6 cm^{-3}, the P12 values for the singlets are all larger than ours by a maximum of 66 per cent, this value being for λ6678, and all smaller than ours by as much as 16.3 per cent for the triplets. A similar trend but of smaller magnitude is seen at 10^4 cm^{-3}. Given that CE from the metastable is increasingly important for higher densities and temperatures, and despite the fact that P12 used Bray et al. (2000) for CE, as did we, these differences are likely to be attributable to unidentified differences in the way that we and P12 calculated the rates for collisional processes among the lower levels.

The emissivities of the earlier P05 model are similar to those of P12, except for the 5876, 6678 Å lines, which were the most affected by the code error previously mentioned (see also Aver et al. 2013).

We mentioned earlier the reasons for preferring the rates of Bray et al. (2000) over those of Sawey & Berrington (1993) and the fact that the Bray et al. (2000) results are also not without weaknesses. In view of this, we consider that it is useful to view the differences between our two $n = 40$ models, PB40 and SB93, that differ only in that they use these different CE rates, as a measure of the uncertainty due to this choice of rate coefficients, and as a way to identify lines that are relatively insensitive to that choice. For example Table A1 shows that the results of PB40 and SB93 for the strongest lines all agree within 1 per cent at 10^2 cm^{-3}, whereas in Table A2 at 10^4 cm^{-3}, eight of the lines, mostly but not exclusively among triplet states, differ by more than 1 per cent

The final column in the emissivity tables (PB + PE + PI) shows the result of adding photoionization and photoexcitation of excited states by a 100 000 K diluted black-body radiation field, in case B. With a dilution factor, $d = 10^{-16}$, we can see that the emissivities of the main lines are very close to those of the PB model. We note that an appropriate dilution factor 0.1 pc from a typical white dwarf would be $\approx 5 \times 10^{-17}$ at which level PE and PI have a negligible effect on the emissivities.

The results of our case B calculation, PB, are available from the CDS on a grid of electron temperatures and densities, $\log_{10} N_e$ (cm^{-3}) = 2.0(0.5)6.0 and $\log_{10} T_e$ (K) = 3.0(0.1)4.6, for all transitions with upper principal quantum number = 2–25 and lower principal quantum number = 2–5. We also provide a small FORTRAN program to make two-dimensional interpolation of the emissivity tables to any desired density and temperature within the tabulated ranges.

4.1 Infrared lines

It is also interesting to compare our PB rates with those calculated by S96 for weaker infrared lines, some of which were observed by Rubin et al. (1998). Table 5 shows such a comparison, for the lines listed by Rubin et al. The authors provide the S96 emissivities (case B) relative to the 4471 Å reference line, calculated for $T_e = 10\,000$ K and $N_e = 10\,000$ cm^{-3}. The emissivity of the reference line in our PB case is about 4 per cent higher than the S96 value. Regarding the infrared lines, in most cases the relative intensities are within 1 per cent our values. However, there are a few notable deviations, particularly the 5d-4f transitions.

Table 5. Emissivities of a selection of infrared lines, as listed in Rubin et al. (1998), and as calculated by S96 (case B) and with the present case B (PB). The wavelengths λ are in vacuum except for 4471 Å that is in air. The values are relative to the 4471 Å emissivity and were calculated for $T_e = 10\,000$ K and $N_e = 10\,000$ cm^{-3}. The cases where the PB values differ from the S96 ones by more than 1 per cent are indicated in brackets. The last column (PBf) indicates our case B values, where the l-changing collision rates have been changed (see text). Changes of more than 1 per cent relative to PB are indicated. The last row gives the fluxes of the 4471 Å line in 10^{-26} erg cm^3 s^{-1}.

λ (μm)	Levels	S96	PB	PBf
2.855 020	T 5p-4s	0.001 71	0.001 71	0.001 71
3.330 851	S 5p-4s	$9.264\ 10^{-4}$	$9.32\ 10^{-4}$	$9.30\ 10^{-4}$
3.703 571	T 5d-4p	0.005 595	0.005 63	0.005 62
4.006 400	S 5p-4d	$4.287\ 10^{-4}$	$4.32\ 10^{-4}$	$4.30\ 10^{-4}$
4.037 735	T 5f-4d	0.027 39	0.0268	0.0270
4.040 934	S 5f-4d	0.009 13	0.008 77 (4 per cent)	0.008 82
4.049014	T 5g-4f	0.075 61	0.0737 (3 per cent)	0.0761 (3 per cent)
4.049 034	S 5g-4f	0.025 20	0.0245 (3 per cent)	0.0253 (3 per cent)
4.054 506	S 5d-4f	7.48×10^{-5}	4.90×10^{-5} (53 per cent)	4.89×10^{-5}
4.056 346	T 5d-4f	2.01×10^{-4}	1.84×10^{-4} (9 per cent)	1.84×10^{-4}
4.122 730	S 5d-4p	0.002 22	0.002 21	0.002 21
4.244 067	T 5p-4d	0.003 12	0.003 12	0.00311
4.606 601	S 5s-4p	$7.479\ 10^{-4}$	$7.83\ 10^{-4}$ (5 per cent)	$7.85\ 10^{-4}$
4.694 980	T 5s-4p	0.001 581	0.001 87 (16 per cent)	0.001 88
0.4471	T 4d-2p	6.16	6.44 (4 per cent)	6.43

As we have previously mentioned, the rates for the electron and proton induced *l*-changing collisions used by P05 and P12 are rather uncertain in that their calculations are based on CLOUDY but Guzmán et al. (2017) present proton rates that are stated to come from CLOUDY, which are too small by a factor of approximately 40. It is not clear whether these rates were used in the P05 and P12 calculations. It is clear, however, that those calculations did use the semiclassical methods of VF01 which grossly underestimate collision rates due to neglect of the quantum mechanical contribution from large impact parameters.

As already shown by Guzmán et al. (2017), the emissivities of the main optical lines change by less than 0.1 per cent, when different electron rates are used, with the exception of the case for a very low $T = 100$ K and a high density of 10^6 cm^{-3}. The same authors showed that variations of about 5 per cent are present in several cases for weaker transitions.

To assess how much *l*-changing collisions affect the infrared lines in the table, we have run our case B model decreasing the electron collision rates by a factor of 6 and also by decreasing the proton ones by a factor of 40, consistent with the values in fig. 1 of Guzmán et al. (2017). The results, shown in the last column of Table 5 (PBf), indicate small variations, at most 3 per cent. However, transitions from higher principal quantum numbers are significantly affected. The effect of dramatically reducing the proton collision rates is to reduce the coupling between the populations of the higher-*l* states and the lower-*l* states, for a given principal quantum number. Since the low-*l* states have the largest radiative decay rates this leads to larger departure coefficients in the reduced rate case for the higher-*l* states and smaller departure coefficients for the lower-*l* states. These effects only appear at intermediate principal quantum number, once the *l*-changing collision rates begin to dominate over radiative rates.

As principal quantum number increases, these effects appear first in the high-l states. For example, for $N_e = 10\,000$ cm^{-3} and $T_e = 10\,000$K and when $l = n - 1$ the reduced rates lead to an 8 per cent population increase at $n = 10$ and an 9 per cent increase at $n = 20$, while for $l = 0$ decreases of a similar magnitude only appear for $n = 40$ and greater. The increases in the high-l state populations are already apparent for $n = 5$ in the 5g-4f transitions in Table 5.

4.2 The Orion nebula model

The case B emissivities usually used to measure the helium abundance are susceptible to opacity effects, as e.g. discussed by Robbins (1968), Porter et al. (2007), and Blagrave et al. (2007). To illustrate this issue, we consider as an example the Orion nebula.

In real nebulae, the stellar incident spectrum would produce PI and PE within all the levels in neutral He. The neutral helium recombination spectrum is obtained by a balance between He^0, He^+, and He^{++}. To approximate the case of a real nebula, and see which spectral lines are more sensitive to the parameters of a real model, we have therefore considered PE within all levels and PI from all levels up to $n = 25$, although the results are the same if only PI from the ground state and the metastable are considered.

For case B, we have set the photoexcitation and de-excitations to the ground state to zero. We do not model the effects of optical depth in lines or continuum.

We have adopted a modelled photoionizing spectrum obtained from the grid of O-star atmospheres by Lanz & Hubeny (2003) to represent the dominating ionizing flux, from Θ^1 Ori C, an O6 star a radius about 9.4 $R_\odot$. We use the model with an effective temperature of 40 000 K and log $g = 4.0$.

We also experimented with a widely used line-blanketed LTE atmosphere model spectrum from Kurucz, calculated with solar abundances, and surface gravity log $g = 4.5$. The results are nearly the same, as this spectrum is very similar to the above, although with much lower spectral resolution. We note that in the visible and infrared the spectra are close to that of a black-body of $T = 40\,000$ K, but the He ground state photoionizing flux below 504 Å is very different. We also note that the photons below the 2600 Å threshold for photoionizing the metastable 2s ^{3}S are important in driving the population of this level, which in turns affects the populations of all the triplets (see e.g. Clegg & Harrington 1989). We have extended the input spectrum above 90 μm with that of a black-body of $T = 40\,000$ K.

Blagrave et al. (2007) report an *HST* STIS observation (STIS-SLIT1C), for which they derive an approximate temperature and density of $T_e = 8000$ K and $N_e = 2500$ cm^{-3}. Table 6 presents in the first column the observed fluxes corrected for reddening and relative to the 4471 Å line. The second and third columns give the results of the CLOUDY model M and the case B (forced model) predictions from Porter et al. (2005, P05), as reported by Blagrave et al. (2007). As pointed out by the above-mentioned previous authors, opacity effects related to the population of the metastable 2s ^{3}S are present. In fact, the decays to this state such as the 3889 and 3188 are significantly overpredicted by the case B approximation (compared to observations), indicating self-absorption. As a consequence, the decays to the 2p ^{3}P (as the 7065 and 4713 Å lines) are strongly underpredicted. As shown by Blagrave et al. (2007), the CLOUDY model, which takes into account (in a simplified way) opacity effects, provides in general emissivities closer to observation. Similar effects (although much reduced in size) are also present in the singlets.

Returning to our model, we list in column six of Table 6 the emissivities calculated with case B, column (PB). As we have seen in previous tables, there is a general agreement with the P05 results, although not at the level that one might expect (we note that the 5876 and 6678 Å lines were the most affected by code errors).

We have then run our case B model with PI and PE and various distances from the ionizing source. Baldwin et al. (1991) estimated that various regions of the Orion nebula range in distance from Θ^1 Ori C between 3×10^{17} and 10^{18} cm, which result in dilution factors of about 2.5×10^{-12} and 2.2×10^{-13}. We show in Table 6 the results of the full model at representative dilutions of 10^{-12} and 10^{-14}. The table clearly indicates which lines are most affected by the varying PI and PE processes. It is worth noting that variations of a few per cent are also seen in the singlets. Also, the values in the table show that for sufficiently large distances we recover virtually the same emissivities as obtained with the standard case B calculation.

Mesa-Delgado et al. (2009, MD09) and Méndez-Delgado et al. (2021, MD21) report high-resolution deep spectroscopic VLT observations of Herbig–Haro objects in the Orion Nebula that also include spectra of the nebula itself. These spectra contain many helium lines beyond the usual strong visible transitions, some from relatively high principal quantum number. For extraction, Méndez-Delgado et al. (2021) divide their slit into four 'cuts', with cut 4 exclusively containing nebular material. Dereddened fluxes for some of the stronger helium lines are listed under MD09 and MD21 in Table 6, accompanied by our case B results calculated at the temperatures and densities derived for the nebular material by the respective authors. For those transitions which are expected to have a negligible contribution from CE or optical depth effects related to the metastable, agreement is generally good or very good especially for MD09. For example, the MD09 intensities for transitions within the singlet states agree with theory within the stated observational errors for all transitions listed in Table 6. The same applies to the 7f-3d and nd-2p triplet transitions for MD09. It is, however, not true for the intensities from MD21, where significant differences are present in some cases. For example, the intensities of the singlet np-2s series fall well below theory and outside the error bars for $n = 3$, 4, and 5 but significantly above theory for $n = 6$ and 7. The nd-2p intensities are also larger than theory and outside the stated error bars for $n = 9$ and 10. However, the very good agreement between theory and the results of MD09 give confidence that the theory is reliable for those transitions where the effects of population in the metastable are not significant. The reason for the less good agreement with theory for MD21 is unclear but given the good agreement with MD09, it seems unlikely to be due to errors in theory. Observed intensities in the singlet np-2s series being below case B predictions could be explained by some np-1s photon escape leading to results tending towards Case A but this effect should get stronger as n increases, while the opposite is observed.

As mentioned above, self-absorption in transitions ending on the 2^{3}S metastable weakens the triplet np-2s series. This makes it difficult to compare observation and theory for individual triplet lines, especially the strongest visible lines. The effect is strongest for the 3p-2s λ3889 transition and leads to an increase in the 3s-2p λ7065 intensity. If we neglect the effect of opacity on the states with $n > 3$, we would expect the combined energy in these two transitions to be the same irrespective of optical depth effects. From Table 6, we find the observed and calculated $I(3889) + I(7065)$ to be 2.81 and 2.88 in case B from the MD09 observations. The corresponding numbers for the MD21 data are 2.68 and 3.03. In the MD09 data the 4p-2s λ3188 intensity is lower than the case B prediction by 8 per cent. If this is due to self-absorption we would expect enhancements in 3d-2p λ5876 and also 3s-2p λ7065. Adding the intensities of all five lines we find an observed value of 6.75 from the MD09 observations and 6.73 from our case B calculations, which is excellent agreement. The corresponding results for the MD21 observations are 6.32 and

Table 6. Emissivities of a selection from the strongest He optical lines. The values are emissiviy ratios relative to the 4471 Å line. The third column gives the FOS-1SW, STIS-SLIT1c observed values, corrected for reddening; the fourth and fifth columns give the results of the CLOUDY model M and the case B predictions from Porter et al. (2005), as reported by Blagrave et al. (2007). Column PB gives our case B solution, while the following ones give the results of the full model with PI and PE, for different dilutions *d*. All model emissivities in columns six, seven, and eight have been calculated for $T_e = 8000$ K and $N_e = 2500$ cm^{-3}. Column nine (MD09) lists VLT observed intensities from Mesa-Delgado et al. (2009) and column 10 (PB) our case B results calculated for $T_e = 8180$ K and $N_e = 2890$ cm^{-3}. Columns 11 (MD21) and 12 (PB) contain corresponding results from the VLT observations of Méndez-Delgado et al. (2021) calculated for $T_e = 8360$ K and $N_e = 5650$ cm^{-3}. For our calculations, we provide the emissivities of the 4471 Å line in 10^{-26} erg cm^3 s^{-1} in brackets.

λ (Å)	Levels	STIS-SLIT1c	CLOUDY	P05	PB	$d = 10^{-12}$	$d = 10^{-14}$	MD09	PB	MD21	PB
2945	T 5p-2s	0.26 ± 0.01	0.290	0.414	0.412	0.605	0.415	–	0.415	–	0.418
3188	T 4p-2s	–	0.441	0.878	0.862	1.197	0.866	0.802	0.875	0.471	0.886
3355	S 7p-2s	–						0.034	0.038	0.056	0.038
3448	S 6p-2s	–						0.056	0.061	0.079	0.061
3554	T 10d-2p	–						0.052	0.054	0.061	0.054
3587	T 9d-2p	–						0.077	0.075	0.081	0.075
3614	S 5p-2s	–						0.101	0.108	0.089	0.108
3634	T 8d-2p	–						0.099	0.108	0.106	0.107
3705	T 7d-2p	–						0.150	0.162	0.159	0.162
3820	T 6d-2p	–						0.262	0.262	0.251	0.262
3889	T 3p-2s	–	0.780	2.315	2.24	2.778	2.238	1.561	2.29	1.150	2.36
3965	S 4p-2s	–	0.206	0.221	0.219	0.214	0.219	0.211	0.221	0.194	0.222
4026	T 5d-2p	–	0.466	0.472	0.470	0.471	0.470	–	0.471	0.462	0.471
4144	S 6d-2p	–						0.065	0.069	0.070	0.069
4388	S 5d-2p	0.105 ± 0.003	0.120	0.125	0.124	0.122	0.125	0.122	0124	0.119	0.124
4471	T 4d-2p	1	1	1	(7.64)	(7.81)	(7.64)	1	(7.38)	1	(7.48)
4713	T 4s-2p	–	0.153	0.103	0.102	0.115	0.102	0.133	0.102	0.142	0.107
4922	S 4d-2p	0.204 ± 0.005	0.258	0.272	0.269	0.264	0.270	0.278	0.269	0.262	0.268
5016	S 3p-2s	0.47 ± 0.01	0.517	0.566	0.558	0.544	0.558	0.548	0.563	0.495	0.567
5876	T 3d-2p	2.90 ± 0.04	2.815	2.789	2.88	2.842	2.880	3.014	2.87	3.033	2.89
6678	S 3d-2p	0.74 ± 0.01	0.737	0.784	0.811	0.791	0.811	0.805	0.804	0.761	0.802
7065	T 3s-2p	1.46 ± 0.02	1.714	0.612	0.560	0.618	0.560	1.247	0.593	1.527	0.671
7281	S 3s-2p	0.148 ± 0.002	0.155	0.151	0.146	0.140	0.147	0.138	0.151	0.136	0.159
10028	T 7f-3d	–						0.046	0.048	0.050	0.048

6.91 but the large difference between observation and theory for the 4p-2s λ3188 transition indicates that this transition is showing strong self-absorption and even higher members of *n*p-2s series would need to be included to make a valid comparison with theory.

5 CONCLUSIONS

Having established in a previous work (Del Zanna et al. 2020) that earlier studies of the He recombination spectrum suffered from various shortcomings, we have built several collisional-radiative models and compared the emissivities of the main spectral lines in neutral He with some of the most widely used values in the literature. We have focused the comparisons on the case B approximation, as in most previous work.

As the requirement on the accuracy of the predicted emissivities is stringent, of the order of 1 per cent, we conclude that there are several problems in the previous studies. A detailed assessment on the reasons why significant (larger than 1 per cent) differences among different models are present is difficult. The adoption of different CE rates clearly has an effect, but the differences between the S96 and B99 models are surprising.

Before the various implementations of different models in CLOUDY, the S96 was the largest recombination model for He. Comparing the results of a reduced model (*LS*-resolved states up to $n = 40$) to a full model, we were able to partially validate the S96 assumption, showing that for most spectral lines within the low-lying states the emissivities are accurate (within 1 per cent) with the reduced model. So for most cases, a larger model is not strictly necessary. Despite this, significant differences with the S96 results are found, especially for a selection of infrared lines.

The latest implementation within CLOUDY, described in P12, used more accurate rates than previous versions, but still included incorrect rates for *l*-changing collisions. Using our models we found that in reality such rates have little effect on the emissivities of the main optical transitions. A similar conclusion was found by Guzmán et al. (2017) when varying the electron collision rates. There is generally excellent agreement between our emissivities and the P12 ones at the lowest densities, irrespective of temperature, where radiative processes dominate the populations but significant discrepancies are present for several transitions for higher densities at all temperatures.

The principal remaining uncertainty in our atomic model is now the choice of CE rate coefficients from the 2 ^{3}S metastable, which becomes increasingly significant as density increases. Of the two most accurate calculations of these coefficients by Sawey & Berrington (1993) and Bray et al. (2000) we have chosen to use the latter but with the caveat that both have weaknesses. We suggest that it is reasonable to view the differences in emissivities resulting from using one or other of these CE calculations as a measure of the uncertainty due to the CE rates. In particular, by comparing our results from the SB93 model with our PB40 model it is possible to identify transitions that are relatively insensitive to the choice of CE rates. Broadly, the relatively weaker intersystem CE rates means that transitions among singlet states are less sensitive than those within the triplets, although there are some CE effects even on the singlets for transitions with an $n = 3$ upper state. Within the triplet states themselves, transitions are preferred where the upper state is not linked to the metastable by an electric dipole transition, such as the *n*d-2p series. The 4f-3d and 5g-4f transitions in the IR are another such example where CE effects are expected to be very small. At the highest density we consider, the differences between emissivities

from the SB93 and PB40 models reach 5 per cent for the λ10830 transition, which is the one most affected by CE.

Aside from the above issues, there is a further major one which has often been overlooked in the literature. The tabulated He emissivities calculated with the unphysical case B forced solution are widely used in astrophysical codes (see e.g. Luridiana, Morisset & Shaw 2015) and in general within the literature to e.g. measure the helium abundance (see e.g. Peimbert et al. 2007; Aver et al. 2013; Izotov et al. 2014; Aver et al. 2015; Peimbert, Peimbert & Luridiana 2016, for some recent examples).

A full analysis should include observed or well-modelled photoionizing radiation fields, updated atomic data, all the PI and PE effects we have included, and solve the full radiative transfer problem including the any nebular expansion, which have a significant effect as shown by Robbins (1968). In some cases, where optical depths are not too great, the sum of the intensities of a subset of the triplet lines can be a useful diagnostic.

However, for those cases where opacity and other effects are negligible, and the case B solution is an acceptable approximation we provide our results in electronic form, including all transitions within $n \leq 5$ and all those between the $n \leq 5$ and $n' \leq 25$ states. We also provide an interpolation program. We note that we have found significant differences between our emissivities and those calculated by S96 for a few infrared transitions, discussed by Rubin et al. (1998). We therefore recommend our emissivities for future studies, and to benchmark any new case B model.

ACKNOWLEDGEMENTS

GDZ acknowledges support from STFC (UK) via the consolidated grants to the atomic astrophysics group (AAG) at DAMTP, University of Cambridge (ST/P000665/1 and ST/T000481/1). We would like to thank N. R. Badnell for useful discussions on the calculations of A-values and rates for *l*-changing electron collisions and the referee for some helpful comments.

DATA AVAILABILITY

The results of our case B calculation, PB, are available from the CDS on a grid of electron temperatures and densities, $\log_{10} N_e$ (cm^{-3}) = 2.0(0.5)6.0 and $\log_{10} T_e$ (K) = 3.0(0.1)4.6, for all transitions with upper principal quantum number = 2–25 and lower principal quantum number = 2–5. We also provide a FORTRAN program to make two-dimensional interpolation of the emissivity tables.

REFERENCES

Almog Y., Netzer H., 1989, MNRAS, 238, 57
Aver E., Olive K. A., Porter R. L., Skillman E. D., 2013, J. Cosmol. Astropart. Phys., 11, 17
Aver E., Olive K. A., Skillman E. D., 2015, J. Cosmol. Astropart. Phys., 7, 11
Badnell N. R., et al., 2021, MNRAS, 507, 2922
Baker J. G., Menzel D. H., 1938, ApJ, 88, 52
Baldwin J. A., Ferland G. J., Martin P. G., Corbin M. R., Cota S. A., Peterson B. M., Slettebak A., 1991, ApJ, 374, 580
Bates D. R., Damgaard A., 1949, Phil. Trans. R. Soc. A, 242, 101
Bauman R. P., Porter R. L., Ferland G. J., MacAdam K. B., 2005, ApJ, 628, 541
Benjamin R. A., Skillman E. D., Smits D. P., 1999, ApJ, 514, 307
Berrington K. A., Kingston A. E., 1987, J. Phys. B At. Mol. Phys., 20, 6631
Blagrave K. P. M., Martin P. G., Rubin R. H., Dufour R. J., Baldwin J. A., Hester J. J., Walter D. K., 2007, ApJ, 655, 299
Bray I., Burgess A., Fursa D. V., Tully J. A., 2000, A&AS, 146, 481
Brocklehurst M., 1972, MNRAS, 157, 211
Burgess A., Seaton M. J., 1960a, MNRAS, 120, 121
Burgess A., Seaton M. J., 1960b, MNRAS, 121, 471
Burgess A., Summers H. P., 1969, ApJ, 157, 1007
Burgess A., Tully J. A., 1992, A&A, 254, 436
Clegg R. E. S., Harrington J. P., 1989, MNRAS, 239, 869
Del Zanna G., Storey P. J., Badnell N. R., Andretta V., 2020, ApJ, 898, 72
Dere K. P., Del Zanna G., Young P. R., Landi E., Sutherland R. S., 2019, ApJS, 241, 22
Drake G. W. F., 1996, Springer Handbook of Atomic, Molecular, and Optical Physics, Vol. 154. Springer, New York, NY
Drake G. W. F., 2006, Springer Handbook of Atomic, Molecular, and Optical Physics. Springer, New York, NY
Drake G. W. F., Morton D. C., 2007, ApJS, 170, 251
Ferland G. J. et al., 2017, Rev. Mex. Astron. Astrofis., 53, 385
Fernley J. A., Seaton M. J., Taylor K. T., 1987, J. Phys. B At. Mol. Phys., 20, 6457
Guzmán F., Badnell N. R., Williams R. J. R., van Hoof P. A. M., Chatzikos M., Ferland G. J., 2017, MNRAS, 464, 312
Hummer D. G., Storey P. J., 1998, MNRAS, 297, 1073
Izotov Y. I., Thuan T. X., Guseva N. G., 2014, MNRAS, 445, 778
Karzas W. J., Latter R., 1961, ApJS, 6, 167
Kono A., Hattori S., 1984, Phys. Rev. A, 29, 2981
Lanz T., Hubeny I., 2003, ApJS, 146, 417
Luridiana V., Morisset C., Shaw R. A., 2015, A&A, 573, A42
Mathis J. S., 1957, ApJ, 125, 318
Méndez-Delgado J. E., Esteban C., García-Rojas J., Henney W. J., Mesa-Delgado A., Arellano-Córdova K. Z., 2021, MNRAS, 502, 1703
Mesa-Delgado A., Esteban C., García-Rojas J., Luridiana V., Bautista M., Rodríguez M., López-Martín L., Peimbert M., 2009, MNRAS, 395, 855
Peimbert A., Peimbert M., Luridiana V., 2016, Rev. Mex. Astron. Astrofis., 52, 419
Peimbert M., Luridiana V., Peimbert A., 2007, ApJ, 666, 636
Pengelly R. M., Seaton M. J., 1964, MNRAS, 127, 165
Percival I. C., Richards D., 1978, MNRAS, 183, 329
Porter R. L., Bauman R. P., Ferland G. J., MacAdam K. B., 2005, ApJ, 622, L73
Porter R. L., Ferland G. J., MacAdam K. B., 2007, ApJ, 657, 327
Porter R. L., Ferland G. J., Storey P. J., Detisch M. J., 2012, MNRAS, 425, L28
Robbins R. R., 1968, ApJ, 151, 511
Robbins R. R., 1970, ApJ, 160, 519
Rubin R. H., Colgan S. W. J., Dufour R. J., Lord S. D., 1998, ApJ, 501, L209
Sawey P. M. J., Berrington K. A., 1993, At. Data Nucl. Data Tables, 55, 81
Seaton M. J., 1960, MNRAS, 120, 326
Seaton M. J., 1962, Proc. Phys. Soc., 79, 1105
Smits D. P., 1991, MNRAS, 248, 193
Smits D. P., 1996, MNRAS, 278, 683
Storey P. J., Hummer D. G., 1991, Comput. Phys. Commun., 66, 129
van Regemorter H., Binh Dy H., Prudhomme M., 1979, J. Phys. B At. Mol. Phys., 12, 1053
Vriens L., Smeets A. H. M., 1980, Phys. Rev. A, 22, 940
Vrinceanu D., Flannery M. R., 2001, Phys. Rev. A, 63, 032701

SUPPORTING INFORMATION

Supplementary data are available at *MNRAS* online.

Please note: Oxford University Press is not responsible for the content or functionality of any supporting materials supplied by the authors. Any queries (other than missing material) should be directed to the corresponding author for the article.

APPENDIX A: OTHER CASES

The following Tables A1–A3 present our line emissivities, compared to earlier work, for T_e = 20 000 K and a range of electron densities. Tables A4–A6 provide the same comparisons for T_e = 5000 K and the same range of densities.

Table A1. Emissivities (10^{-26} erg cm^3 s^{-1}) of the strongest He lines, for $T_e = 20\,000$ K and $N_e = 10^6$ cm^{-3}.

λ (Å)	Levels	Earlier work								Present work		
		B72 (A)	B72 (B)	S96 (A)	S96 (B)	B99 (B)	P05 (B)	P12 (B)	SB93(B)	PB40 (B)	PB (A)	PB (B)
2945	T 5p-2s	1.66	1.66	–	–	1.87	2.11	2.22	2.26	2.27	2.27	2.27
3188	T 4p-2s	3.43	3.43	3.47	3.47	5.47	4.96	5.09	5.87	5.08	5.08	5.09
3889	T 3p-2s	8.30	8.30	8.22	8.22	16.7	14.9	15.0	17.8	16.2	16.2	16.3
3965	S 4p-2s	0.027	0.83		0.81	0.99	1.49	1.21	1.07	1.02	0.034	1.02
4026	T 5d-2p	1.45	1.45	1.44	1.44	1.44	1.90	2.01	2.04	2.05	2.05	2.05
4388	S 5d-2p	0.37	0.38		0.38	0.38	0.47	0.57	0.45	0.45	0.43	0.45
4471	T 4d-2p	2.98	2.98	3.0	3.0	5.58	4.42	4.71	6.01	4.72	4.72	4.72
4713	T 4s-2p	0.41	0.41	0.46	0.46	1.72	1.09	1.05	1.77	1.31	1.31	1.31
4922	S 4d-2p	0.78	0.80	0.76	0.79	1.05	1.03	1.31	1.10	0.97	0.93	0.97
5016	S 3p-2s	0.045	2.04	0.045	1.99	2.71	2.74	3.17	2.87	2.76	0.062	2.76
5876	T 3d-2p	7.62	7.62	7.56	7.56	17.8	16.6	18.3	18.9	17.6	17.6	17.6
6678	S 3d-2p	2.09	2.14	2.05	2.12	2.99	3.25	4.88	3.10	2.93	2.82	2.93
7065	T 3s-2p	1.40	1.40	1.91	1.91	9.15	8.10	7.62	9.40	8.85	8.83	8.85
7281	S 3s-2p	0.33	0.55	0.34	0.58	1.36	1.23	1.30	1.40	1.30	0.99	1.30
10830	T 2p-2s	14.9	14.9	351	351	253	237	215	257	256	256	256
18685	T 4f-3d					1.28	1.32	1.78	1.36	1.25	1.24	1.25
20587	S 2p-2s	2.6×10^{-4}			6.28	5.46	–	5.98	5.33	5.6	6×10^{-3}	5.55

Note. The first column gives the wavelength (in air, except the last ones in vacuum), the second indicates if a line is between singlets (S) or triplets (T). B72 (A): Brocklehurst (1972) case A; B72 (B): Brocklehurst (1972) case B; S96 (A): Smits (1996) case A; S96 (B): Smits (1996) case B; B99(B): Benjamin et al. (1999) case B; P05 (B): Porter et al. (2005) case B; P12 (B): Porter et al. (2012) case B; SB93 (B): $n = 40$ model with SB93 rates, case B; PB40 (B): $n = 40$ model with the Bray et al. rates, case B; PB(A): full $n = 500$ model case A; PB(B): full $n = 500$ model case B.

Table A2. Emissivities (10^{-26} erg cm^3 s^{-1}) of the strongest He lines, for $T_e = 20\,000$ K and $N_e = 10^4$ cm^{-3} case B.

λ (Å)	Levels	Earlier work					Present work	
		B72	S96	B99	P05	P12	PB40	PB
2945	T 5p-2s	1.65	–	1.82	1.99	2.12	2.13	2.13
3188	T 4p-2s	3.41	3.45	5.05	4.58	4.79	4.71	4.71
3889	T 3p-2s	8.22	8.18	14.97	13.3	13.8	14.5	14.5
3965	S 4p-2s	0.82	0.81	0.95	0.97	1.15	0.97	0.97
4026	T 5d-2p	1.43	1.44	1.44	1.78	1.92	1.92	1.92
4388	S 5d-2p	0.38	0.38	0.38	0.45	0.55	0.43	0.43
4471	T 4d-2p	2.95	3.0	5.07	4.08	4.44	4.34	4.35
4713	T 4s-2p	0.41	0.46	1.48	0.96	0.95	1.13	1.13
4922	S 4d-2p	0.80	0.79	0.99	0.97	1.25	0.93	0.93
5016	S 3p-2s	2.03	1.98	2.55	2.55	2.99	2.58	2.58
5876	T 3d-2p	7.60	7.56	15.8	14.8	17.0	15.5	15.5
6678	S 3d-2p	2.15	2.14	2.81	3.08	4.84	2.74	2.74
7065	T 3s-2p	1.40	1.92	7.73	6.81	6.65	7.36	7.36
7281	S 3s-2p	0.55	0.58	1.20	1.09	1.18	1.14	1.14
10830	T 2p-2s	14.8	272.7	206.6	188.4	181	204	204
18685	T 4f-3d	–	–	1.21	1.26	1.78	1.17	1.17
20587	S 2p-2s	–	4.95	4.56	–	5.16	4.50	4.50

Table A3. Emissivities (10^{-26} erg cm^3 s^{-1}) of the strongest He lines, for $T_e = 20\,000$ K and $N_e = 10^2$ cm^{-3} case B.

λ (Å)	Levels	Earlier work					Present work	
		B72	S96	B99	P05	P12	PB40	PB
2945	T 5p-2s	1.65	–	1.68	1.65	1.69	1.68	1.68
3188	T 4p-2s	3.40	3.45	3.53	3.43	3.50	3.48	3.48
3889	T 3p-2s	8.20	8.17	8.53	8.32	8.61	8.59	8.58
3965	S 4p-2s	–	0.80	0.81	0.81	0.84	0.82	0.82
4026	T 5d-2p	1.43	1.44	1.44	1.46	1.48	1.47	1.47
4388	S 5d-2p	–	0.38	0.38	0.38	0.39	0.38	0.38
4471	T 4d-2p	2.94	3.00	3.11	3.01	3.05	3.03	3.03
4713	T 4s-2p	0.41	0.46	0.51	0.48	0.49	0.49	0.49
4922	S 4d-2p	–	0.79	0.80	0.80	0.82	0.80	0.80
5016	S 3p-2s	–	1.97	2.01	2.00	2.06	2.03	2.03
5876	T 3d-2p	7.58	7.56	8.06	7.89	8.13	7.99	8.00
6678	S 3d-2p	–	2.14	2.18	2.17	2.30	2.17	2.18
7065	T 3s-2p	1.40	1.92	2.22	2.15	2.18	2.18	2.18
7281	S 3s-2p	–	0.58	0.61	0.59	0.61	0.61	0.61
10830	T 2p-2s	14.7	25.7	24.6	23.4	23.8	23.7	23.6
18685	T 4f-3d	–	–	0.92	0.96	0.94	0.91	0.92
20587	S 2p-2s	–	2.24	2.24	–	2.29	2.24	2.24

Table A4. Emissivities (10^{-26} erg cm^3 s^{-1}) of the strongest He lines, for T_e = 5000 K and $N_e = 10^6$ cm^{-3} case B.

λ (Å)	Levels	Earlier work					Present work	
		B72	S96	B99	P05	P12	PB40	PB
2945	T 5p-2s	4.30	–	4.36	4.57	4.57	4.36	4.36
3188	T 4p-2s	9.04	9.10	9.18	9.59	9.55	9.12	9.12
3889	T 3p-2s	22.9	22.7	23.3	25.0	24.6	23.6	23.6
3965	S 4p-2s	2.41	2.36	0.95	2.53	2.53	2.41	2.41
4026	T 5d-2p	5.56	5.45	5.47	5.87	5.78	5.57	5.56
4388	S 5d-2p	1.51	1.45	1.46	1.57	1.56	1.49	1.48
4471	T 4d-2p	12.0	12.0	12.1	12.70	12.5	12.0	12.0
4713	T 4s-2p	0.77	0.90	1.48	0.98	0.95	0.94	0.93
4922	S 4d-2p	3.32	3.23	3.25	3.46	3.43	3.26	3.26
5016	S 3p-2s	6.20	6.03	6.11	6.50	6.49	6.15	6.16
5876	T 3d-2p	35.4	34.8	35.3	36.9	37.4	35.1	35.0
6678	S 3d-2p	10.2	10.0	10.1	10.5	10.7	10.0	10.0
7065	T 3s-2p	2.89	4.29	5.19	5.30	5.22	5.05	5.04
7281	S 3s-2p	1.39	1.37	1.46	1.50	1.48	1.43	1.43
10830	T 2p-2s	47.5	245.	234.	214	213	189	189
18685	T 4f-3d	–	–	4.97	5.41	5.35	4.90	4.90
20587	S 2p-2s	–	10.7	10.6	–	10.7	10.1	10.1

Table A5. Emissivities (10^{-26} erg cm^3 s^{-1}) of the strongest He lines, for T_e = 5000 K and $N_e = 10^4$ cm^{-3} case B.

λ (Å)	Levels	Earlier work					Present work	
		B72	S96	B99	P05	P12	PB40	PB
2945	T 5p-2s	4.16	–	4.21	4.26	4.26	4.22	4.22
3188	T 4p-2s	8.76	8.82	8.83	8.95	8.92	8.83	8.82
3889	T 3p-2s	22.2	22.0	22.3	23.3	22.9	22.7	22.7
3965	S 4p-2s	2.33	2.29	2.29	2.35	2.36	2.32	2.32
4026	T 5d-2p	5.38	5.32	5.31	5.43	5.43	5.41	5.41
4388	S 5d-2p	1.46	1.41	1.42	1.45	1.46	1.44	1.44
4471	T 4d-2p	11.7	11.8	11.8	11.8	11.8	11.7	11.7
4713	T 4s-2p	0.76	0.88	0.90	0.93	0.90	0.91	0.91
4922	S 4d-2p	3.23	3.09	3.17	3.22	3.21	3.19	3.19
5016	S 3p-2s	6.00	0.13	5.88	6.04	6.04	5.96	5.96
5876	T 3d-2p	35.3	34.8	35.0	34.4	34.9	35.2	35.2
6678	S 3d-2p	10.2	9.8	10.0	9.9	10.0	10.1	10.1
7065	T 3s-2p	2.85	4.20	4.70	4.75	4.67	4.67	4.66
7281	S 3s-2p	1.26	0.64	1.39	1.39	1.38	1.38	1.39
10830	T 2p-2s	46.4	154	152	140	140	130	130
18685	T 4f-3d	–	–	5.06	5.13	4.99	5.09	5.09
20587	S 2p-2s	–	8.96	8.94	–	8.85	8.82	8.83

Table A6. Emissivities (10^{-26} erg cm^3 s^{-1}) of the strongest He lines, for T_e = 5000 K and $N_e = 10^2$ cm^{-3} case B.

λ (Å)	Levels	Earlier work					Present work	
		B72	S96	B99	P05	P12	PB40	PB
2945	T 5p-2s	4.12	–	4.20	4.14	4.19	4.19	4.17
3188	T 4p-2s	8.66	8.76	8.79	8.69	8.76	8.75	8.72
3889	T 3p-2s	21.9	21.8	22.0	22.5	22.4	22.3	22.3
3965	S 4p-2s	–	2.27	2.28	2.28	2.31	2.30	2.30
4026	T 5d-2p	5.31	5.28	5.31	5.28	5.37	5.35	5.35
4388	S 5d-2p	–	1.41	1.42	1.41	1.44	1.43	1.43
4471	T 4d-2p	11.6	11.74	11.8	11.5	11.6	11.6	11.6
4713	T 4s-2p	0.76	0.88	0.89	0.90	0.89	0.90	0.89
4922	S 4d-2p	–	3.16	3.17	3.13	3.18	3.16	3.16
5016	S 3p-2s	–	5.81	5.85	5.85	5.93	5.89	5.89
5876	T 3d-2p	35.0	34.5	35.3	33.6	34.9	34.9	35.2
6678	S 3d-2p	–	10.05	10.11	9.64	10.0	10.0	10.1
7065	T 3s-2p	2.83	4.18	4.22	4.27	4.24	4.25	4.23
7281	S 3s-2p	–	1.33	1.35	1.32	1.33	1.34	1.33
10830	T 2p-2s	46.0	50.6	50.7	49.9	50.8	50.6	50.6
18685	T 4f-3d	–	–	5.19	5.06	5.07	5.10	5.19
20587	S 2p-2s	–	7.42	7.42	–	7.42	7.45	7.47

This paper has been typeset from a TEX/LATEX file prepared by the author.